HHS Public Access

Author manuscript

Plant J. Author manuscript; available in PMC 2019 December 01.

Published in final edited form as:

Plant J. 2018 December ; 96(5): 1036–1050. doi:10.1111/tpj.14088.

Suppressing Arabidopsis GGLT1 affects growth by reducing the L-galactose content and borate cross-linking of rhamnogalacturonan II

Julien Sechet[1,2,8], **Soe Htwe**[1,2], **Breeanna Urbanowicz**[3], **Abigail Agyeman**[3,6], **Wei Feng**[4], **Toshiki Ishikawa**[5], **Marianne Colomes**[1,2,9], **Kavitha Satish Kumar**[1,2], **Maki Kawai-Yamada**[5], **José R. Dinneny**[4,7], **Malcolm A. O'Neill**[3], and **Jenny C. Mortimer**[1,2,*]

[1]Joint BioEnergy Institute, Emeryville, CA 94608 USA

[2]Biosciences Area, Lawrence Berkeley National Laboratory, Berkeley, CA 94720, USA

[3]Complex Carbohydrate Research Center, The University of Georgia, Athens, GA 30602, USA

[4]Department of Plant Biology, Carnegie Institute for Science, Stanford, CA 94305, USA

[5]Graduate School of Science and Engineering, Saitama University, Saitama 338-8570, Japan

[6]Current address: School of Pharmacy, South University, Savannah, GA 31406, USA

[7]Department of Biology, Stanford University, Stanford, CA 94305, USA

[8]Current address: INRA, Versailles, 78000, France

[9]Current address: Nutribio, Paris 75440, France

Abstract

Boron is a micronutrient that is required for the normal growth and development of vascular plants, but its precise functions remain a subject of debate. One established role for boron is in the cell wall where it forms a diester cross-link between two monomers of the low-abundance pectic polysaccharide rhamnogalacturonan-II (RG-II). The inability of RG-II to properly assemble into a dimer results in the formation of cell walls with abnormal biochemical and biomechanical properties and severely impacts plant productivity. Here, we describe the effects on RG-II structure and cross-linking, and on the growth of plants in which the expression of a GDP-sugar transporter (GONST3/GGLT1) has been reduced. In the *GGLT1* silenced plants the amount of L-galactose in sidechain A of RG-II is reduced by up to 50%. This leads to a reduction in the extent of RG-II cross-linking in the cell walls as well as a reduction in the stability of the dimer in the presence of calcium chelators. The silenced plants have a dwarf phenotype, which is rescued by growth in the presence of increased amounts of boric acid. Similar to the *mur1* mutant, which also disrupts RG-II cross-linking, *GGLT1* silenced plants display a loss of cell-wall integrity under salt stress. We conclude that GGLT1 is likely the primary Golgi GDP-L-galactose transporter, and provides GDP-

*Corresponding author: Jenny C. Mortimer (0000-0001-6624-636X), Biosciences Area, Lawrence Berkeley National Laboratory, Berkeley, CA 94720, USA. jcmortimer@lbl.gov, T: +1-510-486-6627, F: +1-510-486-4252.

The authors declare no conflicts of interest.

L-galactose for RG-II biosynthesis. We propose that the L-galactose residue is critical for RG-II dimerization and for the stability of the borate cross link.

Significance Statement

Rhamnogalacuronan-II (RG-II) is a highly complex pectic polysaccharide that is essential for cell wall function. Here we identify the Golgi GDP-L-galactose transporter, which we name GGLT1, and show that it is necessary for RG-II L-galactosylation, and that this, in turn, is essential for RG-II function and plant viability.

Keywords

Rhamnogalacturonan II; Boron; Nucleotide-Sugar Transporter; Golgi; Pectin

Introduction

In flowering plants, a primary role for boron is to form a diester cross-link between two monomers of rhamnogalacturonan-II (RG-II), a pectic polysaccharide present in the cell walls of all vascular plants (O'Neill et al., 2004). RG-II is a structurally complex domain of pectin (Fig. 1)(Atmodjo et al., 2013), which is comprised of 12 different monosaccharides that are linked together by at least 20 different glycosidic linkages (O'Neill et al., 2004). Nevertheless, its structure is largely conserved in vascular plants (Matsunaga et al., 2004, Pabst et al., 2013). The majority of RG-II exists in the wall as a dimer that is generated by forming a borate diester between the side-chain A D-apiose of two RG-II molecules. The inability of RG-II to properly assemble into a dimer results in the formation of cell walls with abnormal biochemical and biomechanical properties and severely impacts plant productivity. Nevertheless, the mechanisms that drive the interactions between borate and RG-II are poorly understood (Chormova et al., 2014, Funakawa and Miwa, 2015).

There is increasing evidence that altering RG-II structure and cross-linking severely impacts plant growth, development, and viability. To date, the only characterized RG-II biosynthetic enzymes are the RHAMNOGALACTURONAN XYLOSYL TRANSFERASEs (RGXT1-4, CAZy family GT77)(Lombard et al., 2014), which catalyze the transfer of xylose from UDP-xylose to fucose to form α-xylose-(1,3)-fucose *in vitro* (Egelund et al., 2008, Petersen et al., 2009). Inactivation of *RGXT1* and *2* has no discernible effect on plant growth or RG-II structure (Egelund et al., 2006), implying redundancy of function, whereas mutations affecting *RGXT4* lead to root and pollen tube growth defects that are lethal (Fangel et al., 2011, Liu et al., 2011). Mutations that prevent the synthesis of UDP-Api and CMP-Kdo are also lethal and provide further evidence for the essential role of RG-II in plant growth (Delmas et al., 2003, Mølhøj et al., 2003, Ahn et al., 2006, Delmas et al., 2008). In the dwarf Arabidopsis *murus* 1 (*mur1*) mutant L-galactose replaces L-fucose in several cell wall polysaccharides, including RG-II, because the plant is unable to produce GDP-fucose in its shoots as it lacks the GDP-D-mannose-4,6-dehydratase GMD1 (Bonin et al., 1997). This has been shown to result in the incomplete formation of the A sidechain of RG-II, which in turn reduces the stability of the borate cross-linked dimer (Bonin et al., 1997, O'Neill et al., 2001). Thus, the structural integrity of RG-II is likely important for its biological functions.

Pectic and hemicellulosic polysaccharides are synthesized in the Golgi apparatus using activated donor substrates, typically in the form of nucleotide diphosphate linked (NDP-) sugars (Davis et al., 2010). However, most NDP-sugars are synthesized in the cytosol (Bar-Peled and O'Neill, 2011). Thus, NDP-sugar transporters (NSTs) are required to provide substrates for glycan synthesis (Rautengarten et al., 2016). The GOLGI-LOCALIZED NST (GONST) sub-family, which forms part of clade IIIa of the NST/Triose Phosphate Transporter superfamily (Rautengarten et al., 2014), is comprised of 4 members related to GONST1 (At2g13650), the first nucleotide sugar transporter described in Arabidopsis (Baldwin et al., 2001, Handford et al., 2004). The members of this family are the only Arabidopsis NSTs that contain a predicted GDP-binding motif (Handford et al., 2004). Arabidopsis is known to synthesize 4 GDP-linked sugars: GDP-L-fucose, GDP-L-galactose, GDP-D-glucose and GDP-D-mannose. GDP-mannose for the glycosylation of glycosylinositolphosphorylceramides (GIPCs) is transported into the Golgi by GONST1 (Mortimer et al., 2013, Fang et al., 2016), whereas GDP-fucose is transported by GONST4, which has been renamed GDP-FUCOSE TRANSPORTER1 (GFT1) (Rautengarten et al., 2016). No Golgi-localized GDP-L-galactose transporters have been identified to date. GDP-L-galactose is synthesized from GDP-mannose in the cytosol by GDP-mannose epimerase (GME)(Gilbert et al., 2009, Mounet-Gilbert et al., 2016). Most GDP-L-galactose is then converted, via L-galactose, into L-ascorbate (vitamin C), which is important for maintaining redox balance in the cell, particularly under abiotic or biotic stress (Smirnoff, 2000). However, some GDP-L-galactose is required for cell wall polysaccharide synthesis since L-galactose is present in side-chain A of RG-II, in the side-chains of xyloglucan from a limited number of plant species (although not Arabidopsis) (Hantus et al., 1997), and corn bran glucuronoarabinoxylan (Rogowski et al., 2015).

Here, we provide evidence that *GONST3* (At1g76340) likely encodes a Golgi-localized GDP-L-galactose transporter, which we rename *GOLGI GDP-L-GALACTOSE TRANSPORTER1* (*GGLT1*). We used RNAi to suppress *GGLT1* expression in Arabidopsis, since complete loss of *GGLT1* is lethal. Plants with decreased *GGLT1* expression have growth defects, which are rescued by increasing the amount of borate in their growth medium. Chemical analysis of the cell walls of *GGLT1* knock-down plants revealed a substantial reduction in the L-galactose decoration of RG-II, which is correlated with a decrease in the proportion of RG-II dimer in the wall and a decrease in the stability of the crosslink. Our results underscore the importance of RG-II to plant survival, and highlight an unexpectedly critical role for L-galactose in borate cross-linking of this unusual pectic polysaccharide.

Results

Subcellular localization of GGLT1

Publicly available gene expression data reveals that *GGLT1* is a ubiquitously expressed gene, with a level of expression that is slightly lower than *GONST1* and *GFT1* (Handford et al., 2004, Rautengarten et al., 2016).). In an earlier study, the sub-cellular localization of GGLT1 was not determined because tagged *GGLT1* could not be expressed *in vivo* (Handford et al., 2004). To overcome this issue, the full length *GGLT1* coding sequence

tagged with a fluorescent protein was introduced into onion epidermal cells by biolistic transformation. Confocal imaging revealed that the fluorescently-tagged GGLT1 gave a punctate signal that co-localized with a Golgi marker (Lao et al., 2014) (Supplemental Fig. S1).

GGLT1 is essential for plant growth and development

No Arabidopsis lines carrying a T-DNA insertion in the *GGLT1* open reading frame have been reported. A single T-DNA line (SAIL_71_H10), with an insertion 841 bp upstream of the start of transcription was obtained, but we were unable to identify any plants homozygous for the T-DNA insertion despite screening at least 30 different seedlings. Therefore, we took a targeted gene-knockdown approach and generated RNA interference (RNAi) transgenic lines with a hairpin (hp) RNA construct, which specifically targeted *GGLT1*. Forty independent hp*GGLT1* transformants were screened, and 4 were selected for characterization (Fig. 2). These lines all had rosettes which were smaller than the empty vector (EV) control (Fig. 2A).

Quantitative real-time PCR (qPCR) showed that in the rosette leaves of the hpRNAi lines #1 – 3 (Fig. 2B) the levels of *GGLT1* silencing were similar (~80-85% decrease relative to the EV control). These data, together with the lack of T-DNA lines, suggest that stronger suppression of *GGLT1* or null mutants will produce plants that are not viable. The expression of *GFT1*, GGLT1's closest homolog, was not affected in lines #3 and #4 but was decreased by up to 50% in lines #1 and #2 (Fig. 2C).

The monosaccharide compositions of the walls, including fucose, were not significantly altered in any of the hpRNAi lines (Fig. 2D; Supplemental Dataset 1), indicating that their phenotypes do not result from altered fucosylation of cell wall glycans and are thus a consequence of *GGLT1* silencing. Moreover, the shortened petiole phenotype that is characteristic of silenced *GFT1* plants as well as *mur1* plants, which also have cell walls with reduced fucose (Reiter et al., 1993, Rautengarten et al., 2016), was not observed in our *hpGGLT1* knock-down lines (Fig. 2A)

Xyloglucan structure is not altered and GIPC glycosylation is unaffected in hp*GGLT1* plants

L-Galactose replaces L-fucose in the xyloglucan formed by *mur1* and *GFT1*-silenced plants where GDP-fucose synthesis or transport is perturbed (O'Neill et al., 2001, Rautengarten et al., 2016). Since GGLT1 and GFT1 are closely related NSTs, we first determined if xyloglucan fucosylation is altered in hp*GGLT1* (Lerouxel et al., 2002). No differences were discernible in the MALDI-TOF mass spectra of the oligosaccharides generated by enzymatic fragmentation of the xyloglucan from hp*GGLT1* and EV control lines (Supplemental Fig. S2). The presence of fucosylated side-chains, together with no substantial increase in the abundance of galactosylated side-chains in the hp*GGLT1* lines supports our assertion that GDP-fucose transport is unaffected in the silenced plants.

GGLT1 is in the same NST sub-clade as GONST1, which provides GDP-mannose specifically for GIPC glycosylation, as opposed to polysaccharide biosynthesis (Mortimer et al., 2013). Although glycosylation of GIPCs is still poorly understood, it is possible that

other GDP-sugars, in addition to GDP-mannose are required. Therefore, we used thin layer chromatography (TLC, Supplemental Fig. S3) and LC-MS (Supplemental Dataset S2) to determine the GIPC glycan composition of hp*GGLT1*. No major differences were discernible between hp*GGLT1* and EV GIPCs. The overall sphingolipidomic composition was also unchanged (Supplemental Dataset S2). Together, the combined results of these studies show that *GGLT1* does not encode a Golgi-localized protein involved in the transport of GDP-L-fucose or GDP-D-mannose. Thus, we next investigated if the L-galactose content of the wall was altered in the *GGLT1* suppressed lines.

hp*GGLT1* has a specific decrease in RG-II L-galactose.

No significant differences were detected in the wall monosaccharide compositions of leaves from soil-grown EV and hp*GGLT1* lines (Fig. 2D; Supplemental Dataset 1). This is not surprising since in primary cell walls D-galactose is far more abundant than L-galactose (Baydoun and Fry, 1988). Moreover, D-galactose and L-galactose are not separated when the monosaccharide composition of the cell wall is determined by HPAEC-PAD.

RG-II is the only known L-galactose-containing polysaccharide present in wild-type Arabidopsis cell walls, thus we next determined whether the structure of RG-II differed in hp*GGLT1* and EV plants. Material enriched in pectic polysaccharides, including RG-II, was obtained by extracting hp*GGLT1* and EV leaf alcohol insoluble residue (AIR) with ammonium oxalate, a calcium chelator. This material was then treated with endopolygalacturonase (EPG), and the products separated by size exclusion chromatography (SEC) (Fig. 3A). This separates RG-II from RG-I and oligogalacturonides, and also separates the RG-II monomer and dimer. In EV control plants the dimer accounts for 77% of the total RG-II isolated from the wall. Somewhat unexpectedly, the dimer accounts for only 49% of the hp*GGLT1* RG-II, and makes up only 6% of the RG-II in *mur1-1* (Fig. 3A and Supplemental Table S1). This led us to suspect that the ability of the hp*GGLT1* RG-II to form dimers or the stability of those dimers had been altered. The latter notion is supported by our SEC data of the RG-II released by EPG treatment of the AIR (Supplemental Table S2). Under these conditions, in the absence of a chelating agent, the dimer accounted for 97% of the RG-II in the EV control plants (1.2-fold more dimer than in the oxalate fraction), 87% of the RG-II in the hp*GGLT1* lines (1.8-fold more dimer than in oxalate fraction), and 70% of *mur1-1* (12-fold more dimer than in the oxalate fraction). These results, together with data showing that calcium chelators partially convert the RG-II dimer to the monomer (Matoh and Kobayashi, 1998, Fleischer et al., 1999), strongly suggest that both the extent of formation and the stability of the borate cross-link in RG-II is affected in the hp*GGLT1* lines.

The differences in dimer abundance in the EPG and oxalate fractions were most pronounced with *mur1-1* plants. This mutant produces RG-II that lacks L-galactose because its A sidechain is truncated (Pabst et al., 2013), which led us to suspect that the L-galactose content of sidechain A of the RG-II from the hp*GGLT1* lines may also be reduced.

To determine if RG-II structure is indeed altered in the hp*GGLT1* lines we isolated the total RG-II from the silenced and EV plants. Glycosyl residue composition analyses showed that D/L-galactose was reduced by ~35% in the most strongly affected hp*GGLT1* lines (Table 1).

We then treated the RG-II with warm TFA (Pabst et al., 2013) to release side-chains A and B. MALDI-TOF MS analysis showed that a substantial portion of side-chain A from hp*GGLT1* RG-II existed as a heptasaccharide whereas virtually all the A chain from the EV control was present as an octasaccharide (Fig. 3B). The side-chain A produced by hp*GGLT1* and EV plants differ by a mass of 162 Da, corresponding to a hexose residue, which we consider likely to be L-galactose. The side-chain B of RG-II contains a D-galactose residue (see Fig. 1). However, no differences were discernible in the structures of this side-chain from the RG-II of hp*GGLT1* and EV plants (Supplemental Fig. S4). Our structural data provide compelling evidence that the abundance of terminal L-galactose present on side-chain A of RG-II is specifically affected in hp*GGLT1* plants.

To confirm the identity of the missing hexose in side-chain A, the RG-II monomers generated from the hp*GGLT1* and EV plants were treated with a recently identified α-L-galactosidase (CAZY family glycosyl hydrolase (GH) 95) from *Bacteroides thetaiotaomicron* that specifically removes the terminal L-galactose from side-chain A of RG-II (Ndeh et al., 2017). Galactose was the only monosaccharide detected by HPAEC-PAD following hydrolysis of EV control RG-II with the α-L-galactosidase (Fig. 4A). Less galactose was released from the RG-II of the hp*GGLT1* silenced lines, relative to the control (Fig. 4B, C). MALDI-TOF MS analysis of side-chain A, released by mild TFA hydrolysis, following α-L-galactosidase treatment of RG-II monomer revealed that the predominant oligosaccharides (*m/z* 1115, 1129, 1143 and 1157) in the EV control plants correspond to side-chain A lacking L-galactose (Fig. 4D, compare to the untreated EV side-chain A in Fig. 3B). The L-galactose was almost completely removed as only low intensity signals corresponding to L-galactosylated side-chain A were discernible (*m/z* 1277, 1291 and 1305) (Fig. 4D). The mass spectra of side-chain A from both *hpGGLT1* silenced lines are similar to the EV control (Fig. 4E, F), demonstrating that the 162 Da mass difference between the EV control and hp*GGLT1* lines in Fig. 3B is due to the specific loss of L-galactose.

It has been proposed that pectin domains may be linked covalently to each other or to other cell wall components e.g. (Popper and Fry, 2008, Atmodjo et al., 2013, Tan et al., 2013). To investigate whether the altered RG-II structure in the *hpGGLT1* silenced lines had affected other pectic domains, the oxalate cell wall fraction was used to perform immune-dotblots with a panel of antibodies raided against different pectin epitopes (Supplemental Fig, S5). However, no difference was observed between the EV control and the silenced lines. In combination with the monosaccharide composition data (Fig. 2D, Supplemental Dataset 1) and the xyloglucan data (Fig. S2) we conclude that the reduction in GGLT1 expression does not impact non-RG-II polymers.

These data do provide strong evidence that silencing of *GGLT1* leads to a reduction in the abundance of L-galactose on side-chain A of RG-II, and provides additional evidence that the absence of this sugar leads to a decrease in the ability of the RG-II monomer to self-assemble into a borate cross-linked dimer. Moreover this L-galactose-depleted dimer is less stable in the presence of calcium chelators than its wild-type counterpart, a result consistent with the notion that borate and calcium interactions with RG-II are important for plant growth (Matoh and Kobayashi, 1998, Feng et al., 2018).

Complementation of hp*GGLT1* growth phenotypes with borate supplementation.

Several growth phenotypes, including the dwarf phenotype of *mur1*, that have been attributed to defects in RG-II structure and cross-linking have been reported to be rescued by supplementing the growth media with additional borate (O'Neill et al., 2001). To further explore the observed growth phenotypes of the hp*GGLT1* lines (Fig. 2), plants were grown hydroponically to control the availability of all macro- and micro-nutrients, including borate. In low borate media, the hp*GGLT1* lines are severely stressed, and their rosette diameter is ~70% smaller than EV control plants (Fig. 5A, B). However, this phenotype is not observed when the silenced plants are grown in a high borate media (Fig. 5A, C). The amount of borate in the growth media did not impact *GGLT1* expression, thereby excluding a potential effect of borate-deficiency or supplementation on transgene expression and silencing strength (Supplemental Fig. S6). Therefore, we conclude that partial loss of the RG-II L-galactose decoration in hp*GGLT1* reduces the rate of RG-II borate-dependent dimerization, directly affecting plant development.

hp*GGLT1* plants grown in low borate conditions have altered cell wall composition and are more easily saccharified.

Since hp*GGLT1* plants grown in the presence of 1mM boric acid or no added boric acid had different phenotypes, we were curious to know if altering RG-II structure and dimerization in hp*GGLT1* led to changes in other cell wall components. Therefore, we determined the monosaccharide composition of destarched leaf AIR from plants grown under the different borate concentrations (Supplemental Fig. S7). No significant visible differences were discernible in hp*GGLT1* and EV plants grown with 1mM borate (Supplemental Fig. S7D; Supplemental Dataset 1). However, we saw increases in the abundance of several neutral monosaccharides, in particular glucose (Supplemental Fig. S7A; Supplemental Dataset 1) in the walls of plants grown with no added borate. No differences in aniline blue staining of the walls of EV and hp*GGLT1* lines were observed suggesting that the increase in non-cellulosic glucose in plants which appear severely stressed (Fig. 6A) is not due to callose deposition (Supplemental Fig. S8). Finally, we performed Saeman hydrolysis of the TFA-resistant AIR to determine the amount of glucose derived from crystalline cellulose. A substantial increase in cellulose-derived glucose was detected in the hp*GGLT1* lines grown with no added borate (Supplemental Fig. S4B), but not with plants grown under high borate conditions (Supplemental Fig. S4E).

To further investigate the altered cell wall in the hp*GGLT1* plants grown with no added borate, we performed a saccharification assay on the destarched AIR to measure the amount of enzymatically accessible sugars in this material. Following a hot water pretreatment, the samples were treated with a commercial saccharification cocktail of GHs, and the amounts of reducing sugar released after 72h was measured. As expected, given the increase in cell wall glucose (Supplemental Fig. S4A, B), low borate grown hp*GGLT1* plants had a significant increase in the amount of sugars released compared to EV (Supplemental Fig. S4C), a difference that was not seen in high borate growth conditions (Supplemental Fig. S4F).

hpGGLT1 has impaired cell wall integrity sensing in response to salinity stress.

Wall structure is also important for growth under environmental stress (Feng *et al*, 2017) Salinity stress weakens the wall, likely by disrupting pectin cross-linking (Byrt et al., 2018). The FERONIA receptor directly binds pectin, and prevents uncontrolled cell expansion caused by salt stress (Feng et al., 2018). Similar to the *fer* mutant, the root cells of *mur1* burst during growth in the presence of salt, suggesting a role for RG-II cross-linking in allowing roots to recover growth.

We predicted that, since *hpGGLT1* plants have disrupted RG-II, if the FERRONIA model is correct, the roots should show a similar loss of wall integrity as *mur1* when grown in the presence of salt. Indeed, compared to wild type, root cells of *hpGGLT1* plants burst after salt treatment during the growth recovery phase. (Fig. 6; Supplemental Movie S1).

L-ascorbic acid content is increased in leaves of hp*GGLT1* plants.

GDP-L-galactose is formed in the cytosol where it can be converted to L-galactono-1,4-lactone for the synthesis of ascorbic acid (vitamin C) (Dowdle et al., 2007). Thus, a reduction in the activity of a Golgi-localized GDP-L-galactose transporter may lead to increased amounts of cytosolic GDP-L-Gal, thereby increasing the availability of substrate for ascorbic acid formation. Indeed, we found that the hp*GGLT1* lines, contain between 59 and 64% more ascorbate than the EV plants (Fig. 7).

Discussion

Nucleotide sugar transporters regulate the flow of donor substrates into the Golgi for use by GTs. However, predicting the NDP-sugar transported by these enzymes from amino acid sequences alone is challenging. Here, we have provided evidence that GGLT is a GDP-L-galactose transporter, and show that it is required for the production of structurally normal RG-II. Reducing *GGLT1* expression led to a decrease in the L-galactose content of RG-II and a reduction in RG-II dimerization and dimer stability. Growth of the silenced plants are rescued by adding additional borate to the growth medium. Thus, suppressing GGLT provides a unique opportunity to investigate the effects of RGII structural changes on boron requirements for plant growth.

GGLT1 is likely a GDP-L-galactose transporter

Despite multiple reported failures to heterologously express the GGLT1 protein (e.g. (Handford et al., 2004)), we were able to transiently express GGLT1 as a YFP-fusion in onion epidermal cells, and confirm its predicted localization to the Golgi apparatus. Unfortunately, as others have also reported, we were unable to express GGLT1 in yeast to perform biochemical analysis of activity in vitro activity. Therefore, we took an in planta approach to determine the function of GGLT1. GDP-L-galactose lacked a reported NST, and in wild-type Arabidopsis, L-galactose is present only in the pectic polysaccharide RG-II. Analysis of RG-II from hpGGLT1 plants showed that there was a reduction in RG-II dimer formation, which was correlated with a specific loss of the terminal L-galactose present on side-chain A. We did not detect changes to other biopolymers known to use GDP-mannose, GDP-glucose or GDP-fucose.

RG-II dimerization is critical for plant development

We propose that GGLT1, and the L-galactose decoration on RG-II, is essential for plant development and reproduction. This is consistent with previous studies showing that L-galactose is present on sidechain A of all RG-IIs analyzed to date (Voxeur et al., 2011, Pabst et al., 2013, Avci et al., 2018, Wu et al., 2018), with studies suggesting that RG-II is critical for pollen development, pollen germination, and seed development, and that plants with abnormal RG-II exhibit major growth defects (Egelund et al., 2006, Egelund et al., 2008, Gilbert et al., 2009, Petersen et al., 2009, Fangel et al., 2011, Liu et al., 2011, Voxeur et al., 2011). When the plants were grown in the presence of boric acid, their reduced growth phenotype was partially rescued. This was also reported for GME-silenced tomato plants (Gilbert et al., 2009, Voxeur et al., 2011). While a reduction in GME expression affects the biosynthesis of all GDP-linked sugars, as well as ascorbate, the authors suggested that it was the loss of RG-II dimerization that was critical (Voxeur et al., 2011), and our study supports this conclusion.

It should be noted that the rosette morphology of hp*GGLT1* plants is different than that described for *mur1* or hp*GFT1*, which has been suggested to arise from the replacement of RG-II L-fucose with L-galactose leading to the incomplete formation of side-chain A (Pabst et al., 2013). Since plants lacking fucose on xyloglucan or arabinogalactan proteins grow normally, the phenotype had been ascribed to reduced RG-II dimerization because of the altered RG-II structure in *mur1* and hp*GFT1*. Our results suggest that either the phenotype is dependent on the exact nature of the RG-II side-chain modification, or that the “cabbage-like” growth habit of *mur1* and hp*GFT1* results from the loss of fucosylation of another molecule. For example, it has been proposed that fucose is necessary for epidermal growth factor (EGF) domain activation of receptor-like kinases (Wang et al., 2001, Verger et al., 2016), and for promoting DELLA interaction with the brassinosteroid pathway (Zentella et al., 2017).

B-deficiency likely induces stress responses that are impacted when L-galactose transport is disrupted

Boron is an essential micro nutrient that is required for normal plant growth and development, and its availability is important for maintaining plant productivity. Too little results in poor plant growth, but too much is toxic. To date, the major described role for boron is to cross-link RG-II (Kobayashi et al., 1996, O’Neill et al., 2004). This has been shown to impact cell wall tensile strength (Ryden et al., 2003) and porosity (Fleischer et al., 1999). In some species, borate deficiency results in cell wall thickening (as reviewed in (Wang et al., 2015)). In our hands, boron-deficient plants did show an increase in cellulose-derived glucose, as well as some hemicellulose derived sugars, including mannose. A cell wall integrity sensing pathway responsive to salinity stress, and acting via the receptor kinase FER, has recently been described and is thought to act via interaction with pectin (Feng et al., 2018). Here we show that *hpGGLT1* plants display a similar salt-specific loss of cell wall integrity as *fer* and *mur1*. These data suggest that RG-II cross-linking is directly disrupted by salinity, or part of a compensatory feedback loop that is necessary to recover wall strength during acclimation. Such a feedback loop has also been reported in other primary cell wall mutants (Voxeur and Höfte, 2016). Transcriptomic data from plants grown

under boron-deficiency show altered transcript accumulation for polygalacturonases, pectin methylesterases and pectate lyases, all enzymes involved in cell wall remodeling, as well as stress response genes (Camacho-Cristobal et al., 2008, Camacho-Cristobal et al., 2011). The hp*GGLT1* plants will be a useful tool to investigate this process further.

Boron has also been shown to impact catalytic activities of plasma membrane proteins (enzymes or transporters) (Goldbach and Wimmer, 2007), control the transcription of specific gene targets (e.g. the boron transporter NIP5 (Tanaka et al., 2016)), and to affect the homeostasis of oxidative compounds that may alter lipid properties (Shah et al., 2017). More recently, it was proposed that boron may serve as a potential link between RG-II and GIPCs. GIPCs, a heavily glycosylated class of sphingolipids, are major components of the plant plasma membrane. Interestingly, this proposed linkage would provide a physical interaction between the plasma membrane and the cell wall (Voxeur and Fry, 2014), and is promising avenue for future investigation.

Conclusion

Here, we have shown that GGLT1 is a Golgi-localized transporter that likely provides GDP-L-galactose for RG-II biosynthesis. The hp*GGLT1* knockdown lines have strong developmental defects that are correlated with reduced RG-II dimerization and stability. hp*GGLT1* is the first plant with an altered cell wall in which one specific sugar, L-galactose, is altered only in RG-II. Demonstrating the importance of this glycosyl residue for proper RG-II dimer formation and stability provides insight into why RG-II structure is conserved. Thus, we conclude that GGLT1, L-galactose, and structurally-complete RG-II are essential for plant growth and development that could be through cell wall integrity sensing. We believe that the hp*GGLT1* silenced plants provide new tools to investigate further the relationship between RG-II structure and plants response to B deficiency or overexposure.

Materials and Methods

Plant Growth Conditions

Arabidopsis seeds were surface sterilized and sown on solid medium containing 0.5 × Murashige and Skoog (MS) salts and sucrose (1% w/v) (Murashige and Skoog, 1962). Following stratification (48h to 72h, 4°C, in the dark), plates were transferred to a growth room (22°C, 100 to 200 µmol.m^{-2}.s^{-}1, 14 h light/10 h dark, 60% humidity). After 7 d, plants were transferred to soil or grown hydroponically as described below. All experiments were performed on at least three independently grown biological replicates unless otherwise stated. After transfer to soil, plants were grown in chambers at 22°C, 100 to 200 µmol.m^{-2}.s^{-1}, 60% humidity and cultivated under long day (16h light/ 8h dark) or short day conditions (10h light/ 14h dark).

For hydroponic growth, seedlings were transferred to a plug of rockwool substrate and supported in a microfuge tube (with the end removed) in a modified pipette tip box. The tip box was filled with growth medium (see (Simmons et al., 2016) for composition). The boron concentration was adjusted as described in the figure legends by addition of boric acid. After

one week, the plants were transferred to a larger hydroponics system (5 L volume) equipped with an aquarium pump. Plants were harvested 2 weeks after transfer.

Subcellular localization

GGLT1 was PCR amplified (see Supplemental Table S2 for primer sequences used in this study) and inserted in the Gateway™ pDONR™/Zeo vector. The N-terminal YFP fusion was created using the LR Clonase II reaction (Life Technologies) following the manufacturer's protocol. GGLT1-YFP, a *cis*-Golgi marker (α-ManI-49-ECFP) was expressed from the pBullet plasmid as previously reported (Lao et al., 2014). Gold particles were coated with plasmid DNA and biolistically transformed into yellow onion epidermal cells as described (Lao et al., 2014). 16-24 h after particle bombardment, YFP and CFP fluorescence were observed using a Zeiss LSM 710 (Carl Zeiss, http://www.zeiss.com/).

hpRNA production

A hairpin (hP) RNAi construct targeting *GGLT1* expression was obtained using the Gateway® compatible pHELLSGATE12 plasmid (Helliwell and Waterhouse, 2003). A 379 bp PCR amplified *GGLT1* sequence fragment was inserted into pDONR™ 223 using BP clonase. Insertion of this sequence in pHELLSGATE12 in both sense and antisense orientations is made possible using a single LR clonase reaction. After transformation of wild-type (ecotype Col-0) Arabidopsis, seeds were selected on 0.5× MS medium supplemented with 1% (w/v) sucrose and kanamycin (50μg.ml^{-1}). Surviving seedlings were transferred to soil. Homozygous T3 lines were used for all assays. All constructs and seeds generated for this project will be made available via JBEI's Inventory of Composable Elements (https://public-registry.jbei.org/).

Release and isolation of RG-II from AIR of empty vector and *hpGGLT1* lines

To remove starch, AIR (250 mg) was suspended in 25 mL 0.1 M sodium acetate, pH 5.0, containing 0.01% Thimerosal and treated at 55°C overnight with shaking (250 rpm) with a Spirizyme Excel (30 μL; Novozymes, Denmark) and Liquozyme SC DS (150 μL; Novozymes, Denmark). The suspension was then filtered, and the insoluble residue washed with buffer. To solubilize pectin, the de-starched AIRs were resuspended in 25 mL 0.5% ammonium oxalate, pH 5.0 containing 0.01% Thimerosal, and shaken at 250 rpm overnight at room temperature. The slurries were filtered through 50 μm nylon mesh layered over a Whatman Grade GF/A filter, and washed with additional oxalate. Finally, the oxalate-soluble material, which is enriched in pectin, was dialyzed (3500 molecular weight cut off) against deionized water for 2-3 days and lyophilized.

To generate RG-II, solutions of the oxalate-soluble material (20-40 mg) in 50 mM ammonium formate, pH 5 (1 mL) were treated for 16 h at room temperature with endo-polygalacturonase (Megazyme M2, 2 units). The digests were filtered (0.2 μm nylon mesh spin filter) and then portions (200 μL per run) fractionated on a Superdex™ 75 10/300 GL column with refractive index detection (O'Neill et al., 1996). Fractions were collected manually and repeatedly freeze dried to remove ammonium formate.

Side-chains A and B were released by treating RG-II (1 – 2 mg) for 1h at 80 °C with 0.1 M TFA (Pabst et al., 2013). The acid was removed under a flow of air. The reside was then dissolved in water and the acidic oligosaccharides enriched using a Supelclean ENVI Carb cartridge (Supleco) as described (Packer et al., 1998). The oligosaccharides were then analyzed by MALDI-TOF MS in the negative ion mode with a Bruker LT Microflex MALDI-TOF mass spectrometer using a Nafion-coated probe and DHB as the matrix (Jacobs and Dahlman, 2001) and in the positive ion mode using the stainless steel probe with DHB as the matrix.

Expression and purification of recombinant α-L-galactosidase (BT1010) from *Bacteroides thetaiotaomicron*

Recombinant proteins were produced in *Escherichia coli* Tuner™ (DE3) (Novagen) cells harboring BT1010 cloned into pET28a in frame with an N-terminal His_6-tag, and purified as described (Ndeh et al., 2017) with minor modifications. Briefly, cells were cultured at 37°C in Luria-Bertani (LB) medium supplemented with kanamycin (50 μg/mL) to mid-exponential phase (OD_{600nm}=0.6-0.8). Recombinant protein expression was induced by the addition of isopropyl-β-D-1-thiogalactopyranoside (IPTG, 0.1 mM) and allowed to proceed overnight at 16°C. Cells were lysed by sonication, and His^6-tagged BT1010 was purified from cell-free extracts by immobilized metal affinity chromatography (IMAC) using HisPur™ Cobalt Resin (ThermoFisher Scientific, USA). Purified protein was dialyzed against Sodium Acetate (50 mM, pH 5.5) using D-Tube™ Dialyzer Maxi devices (MWCO 6-8 kDa; EMD Millipore, USA) and used directly for enzymatic hydrolysis.

Treatment of RG-II with the α-L-galactosidase (BT1010) from *B. thetaiotaomicron*

The RG-II isolated from the empty vector and hp*GGLT1* lines (1 – 2 mg) was converted to the monomer by treatment for 1h at room temperature with 0.1 M HCl (O'Neill et al., 1996). The solutions were dialyzed (3500 molecular weight cut-off) against deionized water and freeze dried. Solutions (200 μL) of the monomer in NaOAc (25 mM, pH 5) were then treated for 24 h at room temperature with the recombinant α-L-galactosidase (BT1010, 9 μg protein) from *B. thetaiotaomicron (Ndeh et al., 2017)*. Each reaction mixture was desalted using a Dionex OnGuard H cartridge (1 ml, Thermo Fisher) and freeze dried. The desalted material was dissolved in water (200 μL) and an aliquot (10-20 μL) analyzed by HPAEC PAD to confirm that galactose had been released by the α-L-galactosidase. An equal volume of 0.2M TFA was then added to the remaining material and the mixture heated for 1h at 80°C. The cooled solution was concentrated to dryness under a flow of air. The material was dissolved in water and the acidic oligosaccharides enriched using a Supelclean ENVI Carb cartridge (Sigma Aldrich) as described (Packer et al., 1998). The oligosaccharides were then analyzed by MALDI-TOF MS in the negative ion mode using a Nafion-coated probe and DHB as the matrix (Jacobs and Dahlman, 2001).

Immuno-Dot Blots

The oxalate-isolated, pectin rich fraction described above was resuspended in water at a final concentration of 0.5 mg/mL. The samples were then serially diluted using water, 1 μL spotted onto nitrocellulose membrane, and allowed to air dry overnight. The membrane was briefly washed with 1 × phosphate buffered saline (PBS), and then incubated with 5 % (w/v)

non-fat dairy milk (NFDM) dissolved in 1× PBS for 1h at room temperature, with gentle agitation. The membrane was then incubated overnight (4 ℃, gentle agitation) in 5 % (w/v) NFDM in 1× PBS containing the primary antibody (1:300 dilution). Following 3, 5-minute washes in 1× PBS, the membrane was then incubated for 1 h at room temperature (gentle agitation) in 5 % (w/v) NFDM in 1× PBS containing the secondary antibody (horse-radish peroxidase linked anti-rat at 1:5000 dilution). The membrane was then washed in 1× PBS (4 × 5 minutes). The blots were developed Enhanced chemiluminescence (ECL) detection reagent (Bio Rad), according to manufacturer's instructions and visualized using an Imager 600 (Amersham). The primary antibodies were obtained from either Professor Paul Knox, University of Leeds (www.plantprobes.net; LM5, LM6, LM19 and LM20) or Professor Michael Hahn, CCRC, University of Georgia (www.carbosource.net; CCRC-M35) (Jones et al., 1997, Willats et al., 1998, Verhertbruggen et al., 2009, Pattathil et al., 2010). Negative controls (water) and positive controls (commercial preparations of the polysaccharides) were performed alongside.

Cell wall monosaccharide composition

Plant tissue (age and type as specified in the figure legend) was harvested, submerged in 96% (v/v) ethanol, and boiled at 70°C for 30min. Following homogenization using a ball mill (Retsch), the pellet was collected by centrifugation (4000 × *g* for 15min). The pellet was then washed with 100% (v/v) ethanol, twice with chloroform:methanol (2:1), followed by successive washes with 65% (v/v), 80% (v/v), and 100% (v/v) ethanol. The remaining pellet of Alcohol Insoluble Residues (AIR) was dried at 40 °C overnight. To remove starch, the AIR was treated exhaustively with a cocktail of α-amylase, amyloglucosidase and pullulanase as described (Harholt et al., 2006).

The monosaccharide composition of the non-cellulosic fraction was determined by hydrolysis of 100 μg AIR with 2 M trifluoroacetic acid (TFA) for 1 h at 120 °C. After cooling and centrifugation, the supernatant was dried under vacuum, resuspended in 200 μL of water and retained for analysis. To obtain the glucose content of the crystalline cellulose fraction, the TFA-insoluble pellet was washed with water and further hydrolyzed with 72% (v/v) sulfuric acid for 1 h at room temperature. The sulfuric acid was then diluted to 1 M with water, the samples incubated at 100 °C for 3 h and neutralized with $BaCO_3$. All samples were filtered using a 22 μm syringe filter, and quantitated by HPAEC-PAD on a Dionex ICS-5000 instrument (Thermo Fisher Scientific) as described (Fang et al., 2016).

Saccharification Assay

Leaf AIR (2 mg) from hydroponically grown plants, prepared as described above, was mixed with 136 μl of water, agitated at 1400 rpm (30 °C, 30 min), and autoclaved at 120 °C for 1 h. Saccharification was initiated by adding 260 μL of 100 mM sodium citrate buffer pH 5.0 containing 80 μg/mL tetracycline and 0.5% (w/w) Cellic CTec2 cellulase (Novozymes, Davis, CA, USA). After 72 h of incubation at 50 °C with shaking (800 rpm), samples were centrifuged (20,000 × g, 3 min) and 10 μL of the supernatant was collected for measurement of reducing sugars using the 3,5-dinitrosalicylic acid assay and glucose as a standard (Miller, 1959).

Ascorbic acid measurement

The ascorbate content of leaves was measured according to Gautier et al. (2009) (Gautier et al., 2009) with modifications. Frozen tissue (1 g) was homogenized, resuspended in 600 µL of 6% (v/v) trichloroacetic acid, and vortexed until thawed. Following incubation on ice for 15 min, the samples were centrifuged (16,000g, 4 °C, 15 min). The supernatants (20 µL) were placed in individual wells of a microtiter plate containing 20 µL 5 mM DTT (in 0.4 M PO_4 buffer, pH 7.4), and kept for 20 min at 37 °C, before adding 10 µL of 0.5% (w/v) N-ethylmaleimide. After 1 min at 21 °C, 80 µL of color reagent was added (solution A: 31% [w/v] orthophosphoric acid, 4.6% [v/v] trichloroacetic acid, and 0.6% [w/v] $FeCl_2$; solution B: 4% [w/v] 2,2-dipyridyl in 70% [v/v] ethanol; A:B, 2.75:1) and plates were incubated at 37 °C for 40 min. Ascorbic acid standards (0 to 50 nmol) were included to allow quantitation. The plate was scanned at 550 nm using a Spectramax M2 plate reader (Molecular Devices).

Aniline Blue

Rosette leaves were collected and fixed in acetic acid:ethanol 95% (3:1) for 1 h at room temperature. Fixed leaves were then treated with 2 M NaOH for 2h prior to neutralization in 50 mM NaPO4 buffer (pH 6.8) for 10 min, and immersion in aniline blue solution (0.01% w/v in 50 mM NaPO4 pH 6.8) was done overnight. Images were obtained with an epifluorescence microscope (Leica MZ16F).

Extraction and analysis of GIPCs

The sphingolipids content was quantified by LC-MS/MS as described previously (Fang et al., 2016) with modifications. Lyophilized leaves (10 mg) were homogenized and incubated in 800 µL of methanol/1-butanol/1 N KOH (2:3:3) at 50°C for 30 min. The homogenate was acidified by addition of 450 µL of 1 N HCl, and 1 mL of water and 1-butanol was added for phase separation. The organic layer was dried, dissolved in tetrahydrofuran/methanol/water (2:1:2, v/v/v) containing 0.1% formic acid and analyzed by LC-MS/MS. Lipid content was calculated using internal standards (Fang et al., 2016).

For TLC analysis, lyophilized leaves were homogenized and then incubated at 50°C for 15 min in the lower layer of a isopropanol:hexane:water 55:20:25 solution. The supernatant was retained, and the extraction was repeated on the pellet. The combined supernatants were dried under N_2 and resuspended methylamine (33% v/v) in ethanol: water (7:3), and incubated at 50°C for 1 hour. The supernatant was dried under N_2 and resuspended in chloroform:ethanol:ammonia:water (10:60:6:24), and incubated overnight at room temperature. Following anion exchange (Strata X-AW 33µm, Phenomenex) as previously described (Fang et al., 2016), the enriched GIPCs were spotted onto TLC plates and developed in chloroform/ methanol/[4M ammonium hydroxide + 1.8M ammonium acetate] (9:7:2) buffer. The plate was stained first with primuline (10mg/100mL of acetone/water 8:2 (v/v)), a solution that binds to lipids and observed under 460 nm light. The plate was then stained with orcinol (5% v/v sulfuric acid in ethanol) to detect sugars.

Quantitative PCR

RNA was extracted from the leaves of 1-month old plants grown in long-day conditions in soil or in hydroponics (as specified in the figure legend), using the RNeasy RNA Plant kit (Qiagen). A total of 0.5-1 μg RNA was reverse-transcribed into cDNA with Superscript II reverse transcriptase (Thermo Fisher Scientific) and $d(T)_{20}$ oligomers (IDT). To determine *GGLT1* and *GFT1* expression, the resultant cDNA was subsequently used as the template in a qPCR reaction containing 2× QuantiFast SYBR Green PCR Kit Master Mix (Qiagen) (plants grown in soil) or 2× SYBR Select Master Mix (Applied Biosystems) (plants grown hydroponically) and gene specific primers for *GGLT1* and *GFT1*. Expression of *Arabidopsis PP2A* (At1g13320) and a SAND family gene (At2g28390) was quantified (see Supplemental Table S2 for all primer sequences), as they have previously been established as housekeeping genes (Czechowski et al., 2005). The PCR reactions were performed using the CFX96 Touch System real-time PCR detection system (Biorad) and the following thermal profile was used for all PCR reactions: 95 °C for 5 min, 40 cycles of 95 °C for 10 s and 60 °C for 30 s.

Cell Integrity Assays

Live imaging of roots was performed as previously described (Feng et al., 2018). 5-day-old seedlings cultured on 1× MS, 1% (w/v) sucrose pH 5.7 Gelrite media were transferred to media supplemented with 140 mM NaCl in a moisture chamber made from a 60 × 15-mm petri dish (Fisher, AS4052). Bright-field images of the root tip area were captured every 15 minutes from a Leica DMI6000 inverted compound microscope with HC PL APO 10× / 0.4 CS objective (Leica) and LAS software (Leica). Images were then stitched together using ImageJ “Pairwise Stitching” plugin. Cell bursting events were manually quantified from the resulting movies. Events where root cells rapidly lost volume or appeared opaque were quantified as a cell-bursting event.

Supplementary Material

Refer to Web version on PubMed Central for supplementary material.

Acknowledgements:

The authors wish to thank Paul Dupree for helpful discussions.

Funding Contributions:

This work was funded as part of the DOE Joint BioEnergy Institute (http://www.jbei.org) supported by the U. S. Department of Energy, Office of Science, Office of Biological and Environmental Research, through contract DE-AC02-05CH11231 between Lawrence Berkeley National Laboratory and the U. S. Department of Energy (J.S., S.H., M.C., K.S.K., J.C.M.). M.A.O, B.R.U. and A.A were supported by a grant from The Division of Chemical Sciences, Geosciences, and Biosciences, Office of Basic Energy Sciences of the US Department of Energy. We also acknowledge the U.S. Department of Energy-funded Center for Plant and Microbial Complex Carbohydrates (Grant DE-FG02-96ER20220) for equipment support. This work was also supported partially by JSPS KAKENHI 17K15411 to T.I. and 26292190 to M.K.-Y. Funding was provided by grants from the National Science Foundation (NSF) Plant Genome Research Program (IOS 1238202), NIH NIGMS (R01 GM123259-01), and Carnegie Institution for Science Endowment to J.R.D.

References

Ahn JW, Verma R, Kim M, Lee JY, Kim YK, Bang JW, Reiter WD **and** Pai HS (2006) Depletion of UDP-D-apiose/UDP-D-xylose synthases results in rhamnogalacturonan-II deficiency, cell wall thickening, and cell death in higher plants. J Biol Chem, 281, 13708–13716. [PubMed: 16549428] **and**

Atmodjo MA, Hao Z **and** Mohnen D (2013) Evolving views of pectin biosynthesis. Annu Rev Plant Biol, 64, 747–779. [PubMed: 23451775] **and**

Avci U, Pena MJ **and** O'Neill MA (2018) Changes in the abundance of cell wall apiogalacturonan and xylogalacturonan and conservation of rhamnogalacturonan II structure during the diversification of the Lemnoideae. Planta, 247, 953–971. [PubMed: 29288327] **and**

Baldwin TC, Handford MG, Yuseff MI, Orellana A **and** Dupree P (2001) Identification and characterization of GONST1, a Golgi-localized GDP-mannose transporter in Arabidopsis. Plant Cell, 13, 2283–2295. [PubMed: 11595802] **and**

Bar-Peled M **and** O'Neill MA (2011) Plant nucleotide sugar formation, interconversion, and salvage by sugar recycling. Annu Rev Plant Biol, 62, 127–155. [PubMed: 21370975]

Baydoun EAH **and** Fry SC (1988) [2–3H]Mannose Incorporation in Cultured Plant Cells: Investigation of L-Galactose Residues of the Primary Cell Wall. Journal of Plant Physiology, 132, 484–490.

Bonin CP, Potter I, Vanzin GF **and** Reiter WD (1997) The *MUR1* gene of Arabidopsis thaliana encodes an isoform of GDP-D-mannose-4,6-dehydratase, catalyzing the first step in the de novo synthesis of GDP-L-fucose. Proceedings of the National Academy of Sciences of the United States of America, 94, 2085–2090. [PubMed: 9050909] **and**

Camacho-Cristobal JJ, Rexach J **and** Gonzalez-Fontes A (2008) Boron in plants: deficiency and toxicity. Journal of integrative plant biology, 50, 1247–1255. [PubMed: 19017112] **and**

Camacho-Cristobal JJ, Rexach J, Herrera-Rodriguez MB, Navarro-Gochicoa MT **and** Gonzalez-Fontes A (2011) Boron deficiency and transcript level changes. Plant science : an international journal of experimental plant biology, 181, 85–89. [PubMed: 21683871] **and**

Chormova D, Messenger DJ **and** Fry SC (2014) Boron bridging of rhamnogalacturonan-II, monitored by gel electrophoresis, occurs during polysaccharide synthesis and secretion but not post-secretion. Plant J, 77, 534–546. [PubMed: 24320597] **and**

Czechowski T, Stitt M, Altmann T, Udvardi MK **and** Scheible W-R (2005) Genome-Wide Identification and Testing of Superior Reference Genes for Transcript Normalization in Arabidopsis. Plant Physiology, 139, 5–17. [PubMed: 16166256] **and**

Davis J, Brandizzi F, Liepman AH **and** Keegstra K (2010) Arabidopsis mannan synthase CSLA9 and glucan synthase CSLC4 have opposite orientations in the Golgi membrane. Plant J, 64, 1028–1037. [PubMed: 21143682] **and**

Delmas F, Petit J, Joubes J, Seveno M, Paccalet T, Hernould M, Lerouge P, Mouras A **and** Chevalier C (2003) The gene expression and enzyme activity of plant 3-deoxy-D-manno-2-octulosonic acid-8-phosphate synthase are preferentially associated with cell division in a cell cycle-dependent manner. Plant Physiol, 133, 348–360. [PubMed: 12970500] **and**

Delmas F, Seveno M, Northey JG, Hernould M, Lerouge P, McCourt P **and** Chevalier C (2008) The synthesis of the rhamnogalacturonan II component 3-deoxy-D-manno-2-octulosonic acid (Kdo) is required for pollen tube growth and elongation. Journal of experimental botany, 59, 2639–2647. [PubMed: 18503041] **and**

Dowdle J, Ishikawa T, Gatzek S, Rolinski S **and** Smirnoff N (2007) Two genes in Arabidopsis thaliana encoding GDP-L-galactose phosphorylase are required for ascorbate biosynthesis and seedling viability. Plant J, 52, 673–689. [PubMed: 17877701] **and**

Egelund J, Damager I, Faber K, Olsen CE, Ulvskov P **and** Petersen BL (2008) Functional characterisation of a putative rhamnogalacturonan II specific xylosyltransferase. FEBS letters, 582, 3217–3222. [PubMed: 18755189] **and**

Egelund J, Petersen BL, Motawia MS, Damager I, Faik A, Olsen CE, Ishii T, Clausen H, Ulvskov P **and** Geshi N (2006) Arabidopsis thaliana RGXT1 and RGXT2 encode Golgi-localized (1,3)-

alpha-D-xylosyltransferases involved in the synthesis of pectic rhamnogalacturonan-II. Plant Cell, 18, 2593–2607. [PubMed: 17056709] **and**

Fang L, Ishikawa T, Rennie EA, Murawska GM, Lao J, Yan J, Tsai AY, Baidoo EE, Xu J, Keasling JD, Demura T, Kawai-Yamada M, Scheller HV **and** Mortimer JC (2016) Loss of Inositol Phosphorylceramide Sphingolipid Mannosylation Induces Plant Immune Responses and Reduces Cellulose Content in Arabidopsis. Plant Cell, 28, 2991–3004. [PubMed: 27895225] **and**

Fangel JU, Petersen BL, Jensen NB, Willats WG, Bacic A **and** Egelund J (2011) A putative Arabidopsis thaliana glycosyltransferase, At4g01220, which is closely related to three plant cell wall-specific xylosyltransferases, is differentially expressed spatially and temporally. Plant science : an international journal of experimental plant biology, 180, 470–479. [PubMed: 21421394] **and**

Feng W, Kita D, Peaucelle A, Cartwright HN, Doan V, Duan Q, Liu M-C, Maman J, Steinhorst L, Schmitz-Thom I, Yvon R, Kudla J, Wu H-M, Cheung AY **and** Dinneny JR (2018) The FERONIA Receptor Kinase Maintains Cell-Wall Integrity during Salt Stress through Ca2+ Signaling. Current Biology, 28, 666–675.e665. [PubMed: 29456142] **and**

Fleischer A, O'Neill MA **and** Ehwald R (1999) The Pore Size of Non-Graminaceous Plant Cell Walls Is Rapidly Decreased by Borate Ester Cross-Linking of the Pectic Polysaccharide Rhamnogalacturonan II. Plant Physiol, 121, 829–838. [PubMed: 10557231] **and**

Funakawa H **and** Miwa K (2015) Synthesis of borate cross-linked rhamnogalacturonan II. Front Plant Sci, 6, 223. [PubMed: 25954281]

Gautier H, Massot C, Stevens R, Serino S **and** Genard M (2009) Regulation of tomato fruit ascorbate content is more highly dependent on fruit irradiance than leaf irradiance. Annals of Botany, 103, 495–504. [PubMed: 19033285] **and**

Gilbert L, Alhagdow M, Nunes-Nesi A, Quemener B, Guillon F, Bouchet B, Faurobert M, Gouble B, Page D, Garcia V, Petit J, Stevens R, Causse M, Fernie AR, Lahaye M, Rothan C **and** Baldet P (2009) GDP-D-mannose 3,5-epimerase (GME) plays a key role at the intersection of ascorbate and non-cellulosic cell-wall biosynthesis in tomato. Plant J, 60, 499–508. [PubMed: 19619161] **and**

Goldbach HE **and** Wimmer MA (2007) Boron in plants and animals: Is there a role beyond cell-wall structure? Journal of Plant Nutrition and Soil Science, 170, 39–48.

Handford MG, Sicilia F, Brandizzi F, Chung JH **and** Dupree P (2004) *Arabidopsis thaliana* expresses multiple Golgi-localised nucleotide-sugar transporters related to GONST1. Mol Genet Genomics, 272, 397–410. [PubMed: 15480787] **and**

Hantus S, Pauly M, Darvill AG, Albersheim P **and** York WS (1997) Structural characterization of novel L-galactose-containing oligosaccharide subunits of jojoba seed xyloglucans. Carbohydrate research, 304, 11–20. [PubMed: 9403992] **and**

Harholt J, Jensen JK, Sorensen SO, Orfila C, Pauly M **and** Scheller HV (2006) ARABINAN DEFICIENT 1 is a putative arabinosyltransferase involved in biosynthesis of pectic arabinan in Arabidopsis. Plant Physiol, 140, 49–58. [PubMed: 16377743] **and**

Helliwell C **and** Waterhouse P (2003) Constructs and methods for high-throughput gene silencing in plants. Methods (San Diego, Calif.), 30, 289–295.

Jacobs A **and** Dahlman O (2001) Enhancement of the quality of MALDI mass spectra of highly acidic oligosaccharides by using a nafion-coated probe. Analytical chemistry, 73, 405–410. [PubMed: 11217739]

Jones L, Seymour GB **and** Knox JP (1997) Localization of Pectic Galactan in Tomato Cell Walls Using a Monoclonal Antibody Specific to (1[->]4)-[beta]-D-Galactan. Plant Physiol, 113, 1405–1412. [PubMed: 12223681] **and**

Kobayashi M, Matoh T **and** Azuma J (1996) Two Chains of Rhamnogalacturonan II Are Cross-Linked by Borate-Diol Ester Bonds in Higher Plant Cell Walls. Plant Physiol, 110, 1017–1020. [PubMed: 12226238] **and**

Lao J, Oikawa A, Bromley JR, McInerney P, Suttangkakul A, Smith-Moritz AM, Plahar H, Chiu TY, Gonzalez Fernandez-Nino SM, Ebert B, Yang F, Christiansen KM, Hansen SF, Stonebloom S, Adams PD, Ronald PC, Hillson NJ, Hadi MZ, Vega-Sanchez ME, Loque D, Scheller HV **and** Heazlewood JL (2014) The plant glycosyltransferase clone collection for functional genomics. Plant Journal, 79, 517–529. [PubMed: 24905498] **and**

Lerouxel O, Choo TS, Seveno M, Usadel B, Faye L, Lerouge P **and** Pauly M (2002) Rapid structural phenotyping of plant cell wall mutants by enzymatic oligosaccharide fingerprinting. Plant Physiol, 130, 1754–1763. [PubMed: 12481058] **and**

Liu X-L, Liu L, Niu Q-K, Xia C, Yang K-Z, Li R, Chen L-Q, Zhang X-Q, Zhou Y **and** Ye D (2011) MALE GAMETOPHYTE DEFECTIVE 4 encodes a rhamnogalacturonan II xylosyltransferase and is important for growth of pollen tubes and roots in Arabidopsis. The Plant Journal, 65, 647–660. [PubMed: 21288267] **and**

Lombard V, Golaconda Ramulu H, Drula E, Coutinho PM **and** Henrissat B (2014) The carbohydrate-active enzymes database (CAZy) in 2013. Nucleic Acids Res, 42, D490–495. [PubMed: 24270786] **and**

Matoh T **and** Kobayashi M (1998) Boron and calcium, essential inorganic constituents of pectic polysaccharides in higher plant cell walls. Journal of Plant Research, 111, 179–190.

Matsunaga T, Ishii T, Matsumoto S, Higuchi M, Darvill A, Albersheim P **and** O'Neill MA (2004) Occurrence of the primary cell wall polysaccharide rhamnogalacturonan II in pteridophytes, lycophytes, and bryophytes. Implications for the evolution of vascular plants. Plant Physiol, 134, 339–351. [PubMed: 14671014] **and**

Miller GL (1959) Use of Dinitrosalicylic Acid Reagent for Determination of Reducing Sugar. Analytical chemistry, 31, 426–428.

Mølhøj M, Verma R **and** Reiter W-D (2003) The biosynthesis of the branched-chain sugar d-apiose in plants: functional cloning and characterization of a UDP-d-apiose/UDP-d-xylose synthase from Arabidopsis. The Plant Journal, 35, 693–703. [PubMed: 12969423] **and**

Mortimer JC, Yu X, Albrecht S, Sicilia F, Huichalaf M, Ampuero D, Michaelson LV, Murphy AM, Matsunaga T, Kurz S, Stephens E, Baldwin TC, Ishii T, Napier JA, Weber AP, Handford MG **and** Dupree P (2013) Abnormal glycosphingolipid mannosylation triggers salicylic acid-mediated responses in Arabidopsis. Plant Cell, 25, 1881–1894. [PubMed: 23695979] **and**

Mounet-Gilbert L, Dumont M, Ferrand C, Bournonville C, Monier A, Jorly J, Lemaire-Chamley M, Mori K, Atienza I, Hernould M, Stevens R, Lehner A, Mollet JC, Rothan C, Lerouge P **and** Baldet P (2016) Two tomato GDP-D-mannose epimerase isoforms involved in ascorbate biosynthesis play specific roles in cell wall biosynthesis and development. Journal of experimental botany, 67, 4767–4777. [PubMed: 27382114] **and**

Murashige T **and** Skoog F (1962) A Revised Medium for Rapid Growth and Bio Assays with Tobacco Tissue Cultures. Physiologia Plantarum, 15, 473–497.

Ndeh D, Rogowski A, Cartmell A, Luis AS, Baslé A, Gray J, Venditto I, Briggs J, Zhang X, Labourel A, Terrapon N, Buffetto F, Nepogodiev S, Xiao Y, Field RA, Zhu Y, O'Neill MA, Urbanowicz BR, York WS, Davies GJ, Abbott DW, Ralet M-C, Martens EC, Henrissat B **and** Gilbert HJ (2017) Complex pectin metabolism by gut bacteria reveals novel catalytic functions. Nature, 544, 65–70. [PubMed: 28329766] **and**

O'Neill MA, Eberhard S, Albersheim P **and** Darvill AG (2001) Requirement of borate cross-linking of cell wall rhamnogalacturonan II for Arabidopsis growth. Science, 294, 846–849. [PubMed: 11679668] **and**

O'Neill MA, Ishii T, Albersheim P **and** Darvill AG (2004) Rhamnogalacturonan II: structure and function of a borate cross-linked cell wall pectic polysaccharide. Annual Review of Plant Biology, 55, 109–139.**and**

O'Neill MA, Warrenfeltz D, Kates K, Pellerin P, Doco T, Darvill AG **and** Albersheim P (1996) Rhamnogalacturonan-II, a pectic polysaccharide in the walls of growing plant cell, forms a dimer that is covalently cross-linked by a borate ester. In vitro conditions for the formation and hydrolysis of the dimer. J Biol Chem, 271, 22923–22930. [PubMed: 8798473] **and**

Pabst M, Fischl RM, Brecker L, Morelle W, Fauland A, Kofeler H, Altmann F **and** Leonard R (2013) Rhamnogalacturonan II structure shows variation in the side chains monosaccharide composition and methylation status within and across different plant species. Plant J, 76, 61–72. [PubMed: 23802881] **and**

Packer NH, Lawson MA, Jardine DR **and** Redmond JW (1998) A general approach to desalting oligosaccharides released from glycoproteins. Glycoconj J, 15, 737–747. [PubMed: 9870349] **and**

Pattathil S, Avci U, Baldwin D, Swennes AG, McGill JA, Popper Z, Bootten T, Albert A, Davis RH, Chennareddy C, Dong R, O'Shea B, Rossi R, Leoff C, Freshour G, Narra R, O'Neil M, York WS **and** Hahn MG (2010) A comprehensive toolkit of plant cell wall glycan-directed monoclonal antibodies. Plant Physiol, 153, 514–525. [PubMed: 20363856] **and**

Petersen BL, Egelund J, Damager I, Faber K, Krüger Jensen J, Yang Z, Bennett EP, Scheller HV **and** Ulvskov P (2009) Assay and heterologous expression in Pichia pastoris of plant cell wall type-II membrane anchored glycosyltransferases. Glycoconjugate Journal, 26, 1235. [PubMed: 19455420] **and**

Popper ZA **and** Fry SC (2008) Xyloglucan-pectin linkages are formed intra-protoplasmically, contribute to wall-assembly, and remain stable in the cell wall. Planta, 227, 781–794. [PubMed: 17987313]

Rautengarten C, Ebert B, Liu L, Stonebloom S, Smith-Moritz AM, Pauly M, Orellana A, Scheller HV **and** Heazlewood JL (2016) The Arabidopsis Golgi-localized GDP-L-fucose transporter is required for plant development. Nat Commun, 7, 12119. [PubMed: 27381418] **and**

Rautengarten C, Ebert B, Moreno I, Temple H, Herter T, Link B, Donas-Cofre D, Moreno A, Saez-Aguayo S, Blanco F, Mortimer JC, Schultink A, Reiter WD, Dupree P, Pauly M, Heazlewood JL, Scheller HV **and** Orellana A (2014) The Golgi localized bifunctional UDP-rhamnose/UDP-galactose transporter family of Arabidopsis. Proc Natl Acad Sci U S A, 111, 11563–11568. [PubMed: 25053812] **and**

Reiter WD, Chapple CC **and** Somerville CR (1993) Altered growth and cell walls in a fucose-deficient mutant of Arabidopsis. Science, 261, 1032–1035. [PubMed: 17739625] **and**

Rogowski A, Briggs JA, Mortimer JC, Tryfona T, Terrapon N, Lowe EC, Basle A, Morland C, Day AM, Zheng H, Rogers TE, Thompson P, Hawkins AR, Yadav MP, Henrissat B, Martens EC, Dupree P, Gilbert HJ **and** Bolam DN (2015) Glycan complexity dictates microbial resource allocation in the large intestine. Nat Commun, 6, 7481. [PubMed: 26112186] **and**

Ryden P, Sugimoto-Shirasu K, Smith AC, Findlay K, Reiter WD **and** McCann MC (2003) Tensile properties of Arabidopsis cell walls depend on both a xyloglucan cross-linked microfibrillar network and rhamnogalacturonan II-borate complexes. Plant Physiol, 132, 1033–1040. [PubMed: 12805631] **and**

Shah A, Wu X, Ullah A, Fahad S, Muhammad R, Yan L **and** Jiang C (2017) Deficiency and toxicity of boron: Alterations in growth, oxidative damage and uptake by citrange orange plants. Ecotoxicology and environmental safety, 145, 575–582. [PubMed: 28800533] **and**

Simmons TJ, Mortimer JC, Bernardinelli OD, Poppler AC, Brown SP, deAzevedo ER, Dupree R **and** Dupree P (2016) Folding of xylan onto cellulose fibrils in plant cell walls revealed by solid-state NMR. Nat Commun, 7, 13902. [PubMed: 28000667] **and**

Smirnoff N (2000) Ascorbate biosynthesis and function in photoprotection. Philosophical Transactions of the Royal Society B: Biological Sciences, 355, 1455–1464.

Tan L, Eberhard S, Pattathil S, Warder C, Glushka J, Yuan C, Hao Z, Zhu X, Avci U, Miller JS, Baldwin D, Pham C, Orlando R, Darvill A, Hahn MG, Kieliszewski MJ **and** Mohnen D (2013) An Arabidopsis cell wall proteoglycan consists of pectin and arabinoxylan covalently linked to an arabinogalactan protein. Plant Cell, 25, 270–287. [PubMed: 23371948] **and**

Tanaka M, Sotta N, Yamazumi Y, Yamashita Y, Miwa K, Murota K, Chiba Y, Hirai MY, Akiyama T, Onouchi H, Naito S **and** Fujiwara T (2016) The Minimum Open Reading Frame, AUG-Stop, Induces Boron-Dependent Ribosome Stalling and mRNA Degradation. The Plant Cell.**and**

Varki A, Cummings RD, Aebi M, Packer NH, Seeberger PH, Esko JD, Stanley P, Hart G, Darvill A, Kinoshita T, Prestegard JJ, Schnaar RL, Freeze HH, Marth JD, Bertozzi CR, Etzler ME, Frank M, Vliegenthart JF, Lutteke T, Perez S, Bolton E, Rudd P, Paulson J, Kanehisa M, Toukach P, Aoki-Kinoshita KF, Dell A, Narimatsu H, York W, Taniguchi N **and** Kornfeld S (2015) Symbol Nomenclature for Graphical Representations of Glycans. Glycobiology, 25, 1323–1324. [PubMed: 26543186] **and**

Verger S, Chabout S, Gineau E **and** Mouille G (2016) Cell adhesion in plants is under the control of putative O-fucosyltransferases. Development (Cambridge, England), 143, 2536–2540.**and**

Verhertbruggen Y, Marcus SE, Haeger A, Ordaz-Ortiz JJ **and** Knox JP (2009) An extended set of monoclonal antibodies to pectic homogalacturonan. Carbohydrate research, 344, 1858–1862. [PubMed: 19144326] **and**

Voxeur A **and** Fry SC (2014) Glycosylinositol phosphorylceramides from Rosa cell cultures are boron-bridged in the plasma membrane and form complexes with rhamnogalacturonan II. Plant J, 79, 139–149. [PubMed: 24804932]

Voxeur A, Gilbert L, Rihouey C, Driouich A, Rothan C, Baldet P **and** Lerouge P (2011) Silencing of the GDP-D-mannose 3,5-epimerase affects the structure and cross-linking of the pectic polysaccharide rhamnogalacturonan II and plant growth in tomato. J Biol Chem, 286, 8014–8020. [PubMed: 21224383] **and**

Voxeur A **and** Höfte H (2016) Cell wall integrity signaling in plants: "To grow or not to grow that's the question". Glycobiology, 26, 950–960. [PubMed: 26945038]

Wang N, Yang C, Pan Z, Liu Y **and** Peng S.a. (2015) Boron deficiency in woody plants: various responses and tolerance mechanisms. Frontiers in plant science, 6.**and**

Wang Y, Shao L, Shi S, Harris RJ, Spellman MW, Stanley P **and** Haltiwanger RS (2001) Modification of epidermal growth factor-like repeats with O-fucose. Molecular cloning and expression of a novel GDP-fucose protein O-fucosyltransferase. J Biol Chem, 276, 40338–40345. [PubMed: 11524432] **and**

Willats WG, Marcus SE **and** Knox JP (1998) Generation of monoclonal antibody specific to (1-->5)-alpha-L-arabinan. Carbohydrate research, 308, 149–152. [PubMed: 9675359] **and**

Wu D, Cui L, Yang G, Ning X, Sun L **and** Zhou Y (2018) Preparing rhamnogalacturonan II domains from seven plant pectins using Penicillium oxalicum degradation and their structural comparison. Carbohydrate Polymers, 180, 209–215. [PubMed: 29103497] **and**

Zentella R, Sui N, Barnhill B, Hsieh WP, Hu J, Shabanowitz J, Boyce M, Olszewski NE, Zhou P, Hunt DF **and** Sun TP (2017) The Arabidopsis O-fucosyltransferase SPINDLY activates nuclear growth repressor DELLA. Nat Chem Biol, 13, 479–485. [PubMed: 28244988] **and**

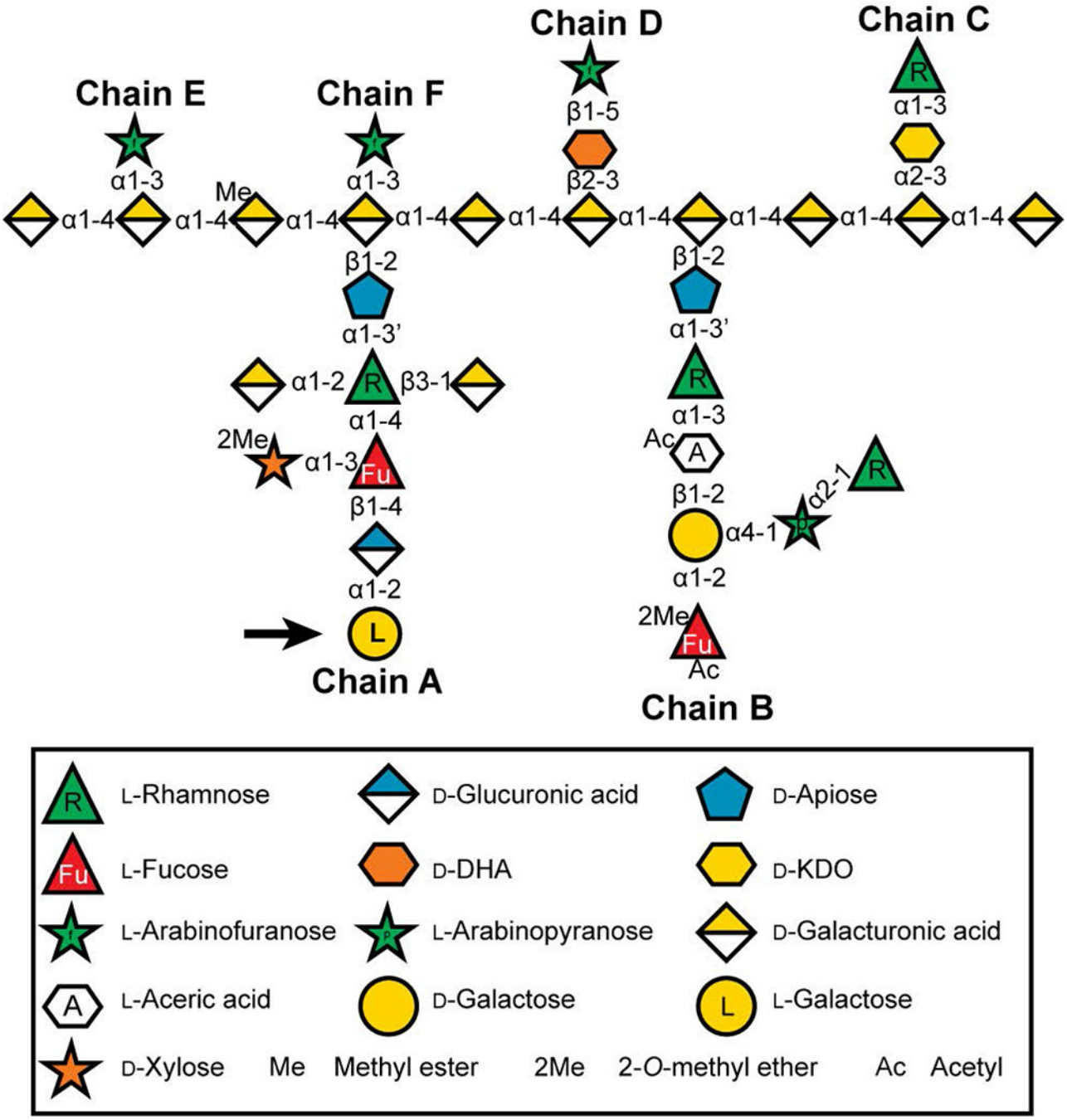

Figure 1: The glycosyl sequence of Arabidopsis RG-II.

Modified from (Ndeh et al., 2017). Sugars are represented using the Symbol Nomenclature for Glycans (SNFG (Varki et al., 2015)), with minor modifications to enable color-blind readers to distinguish L-fucose and L-rhamnose, and with a white hexagon to represent aceric acid since it does not currently have an SNFG designation. D-KDO, 3-deoxy-D-manno-octulosonic acid; D-DHA, 2-keto-3-deoxy-D-lyxo-heptulosaric acid. The L-galactose residue, which is reduced in the *hpGGLT1* lines described in this publication, is marked with an arrow.

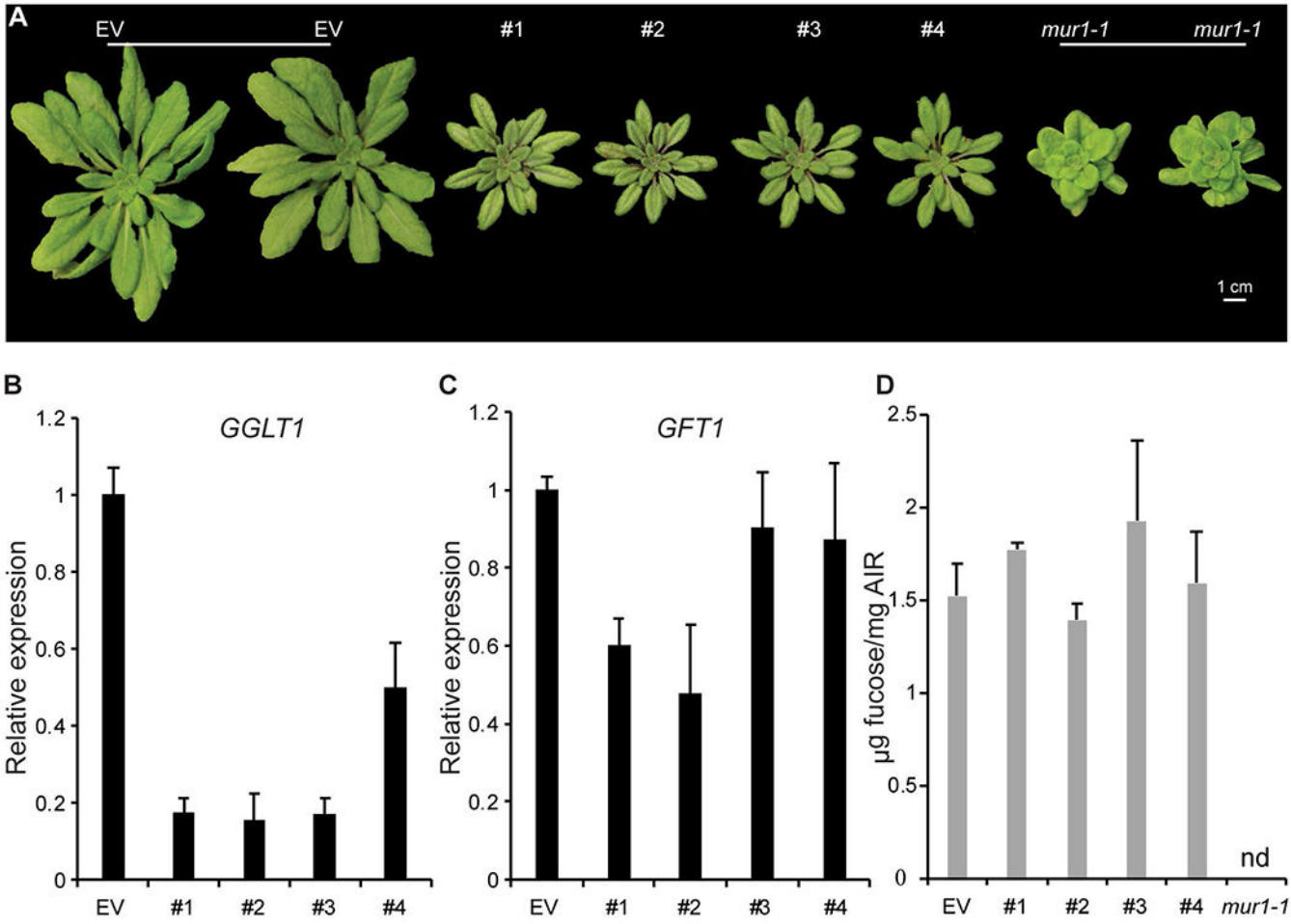

Figure 2: Characterization of hp*GGLT1*:

(A) Empty vector control (EV) and four *hpGGLT1* lines grown on soil for 1 month. (B) Relative expression of *GGLT1* and (C) its closest homologue, *GFT1*, in the four hpRNAi lines selected determined by Q-PCR. (D) The cell wall fucose content of the selected lines. AIR was hydrolyzed with 2M TFA, and the released monosaccharides analyzed by HPAEC-PAD. See Supplemental Data Set 2 for complete data. Data are the mean of 3 biological replicates, error bars are the standard deviation.

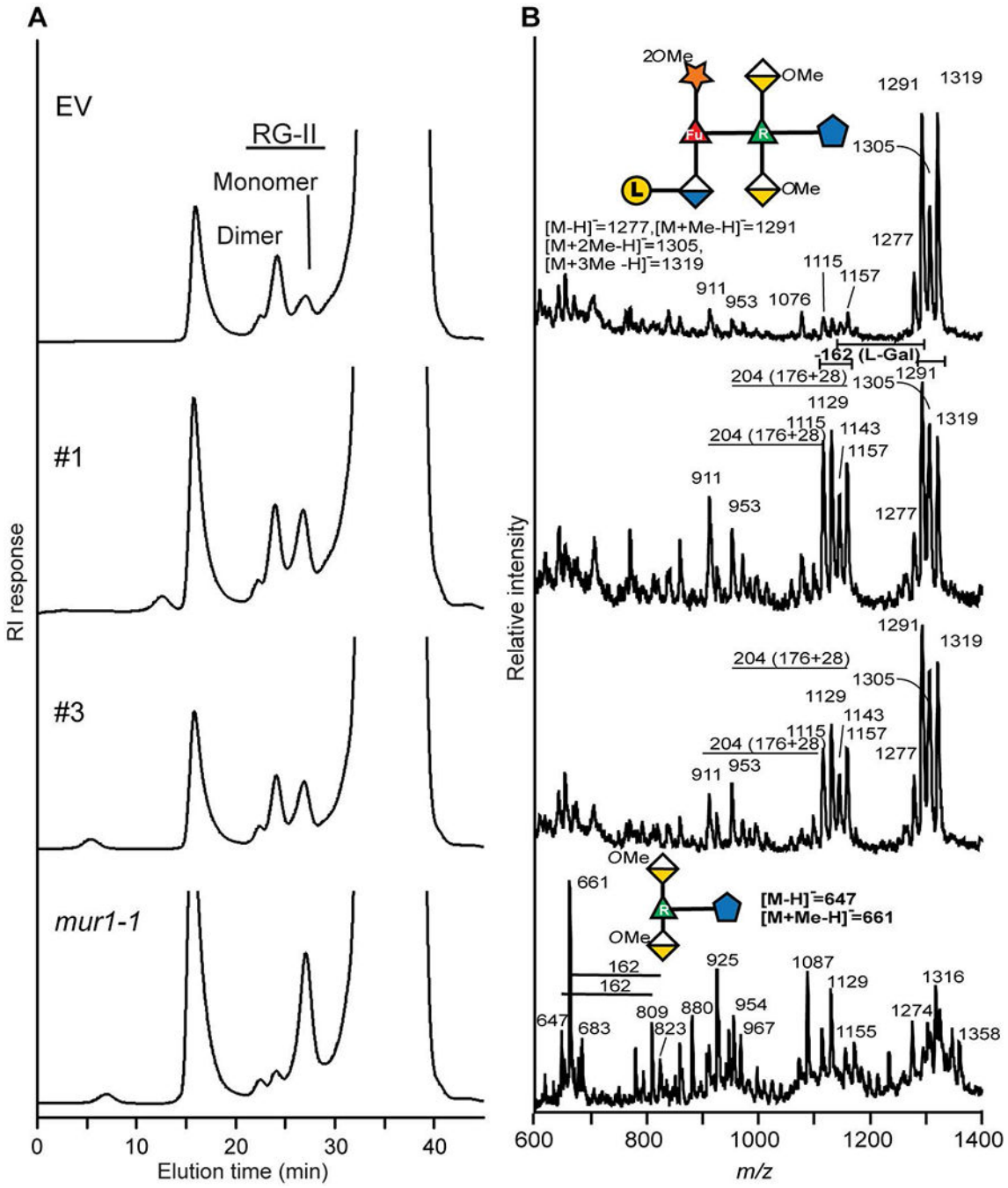

Figure 3: Borate cross-linking of RG-II is reduced in the hp*GGLT1* lines.

(A) The SEC profiles of the material generated by EPG treatment of the oxalate-soluble materials from the AIR of EV control, hp*GGLT1* lines and *mur1-1*. The positions of the RG-II monomer and dimer are shown. (B) The negative ion MALDI-TOF mass spectrum of side-chain A generated by selective acid hydrolysis of RG-II. The predominant oligosaccharide (*m/z* 1277, 1291, 1305, and 1319) in the empty vector corresponds to side-chain A. In the hp*GGLT1* lines between 30 and 50% of side-chain A lacks a hexose (*m/z* 1115, 1129, 1143, and 1157). The mass difference of 14 Da corresponds to differences in the

extent of *O*-methylation of side-chain A. As previously reported (O'Neill et al., 2001) *mur1-1* RG-II contains little if any intact side-chain A. The oligosaccharides structures are represented using a modified SNFG nomenclature. See Figure 1 for details.

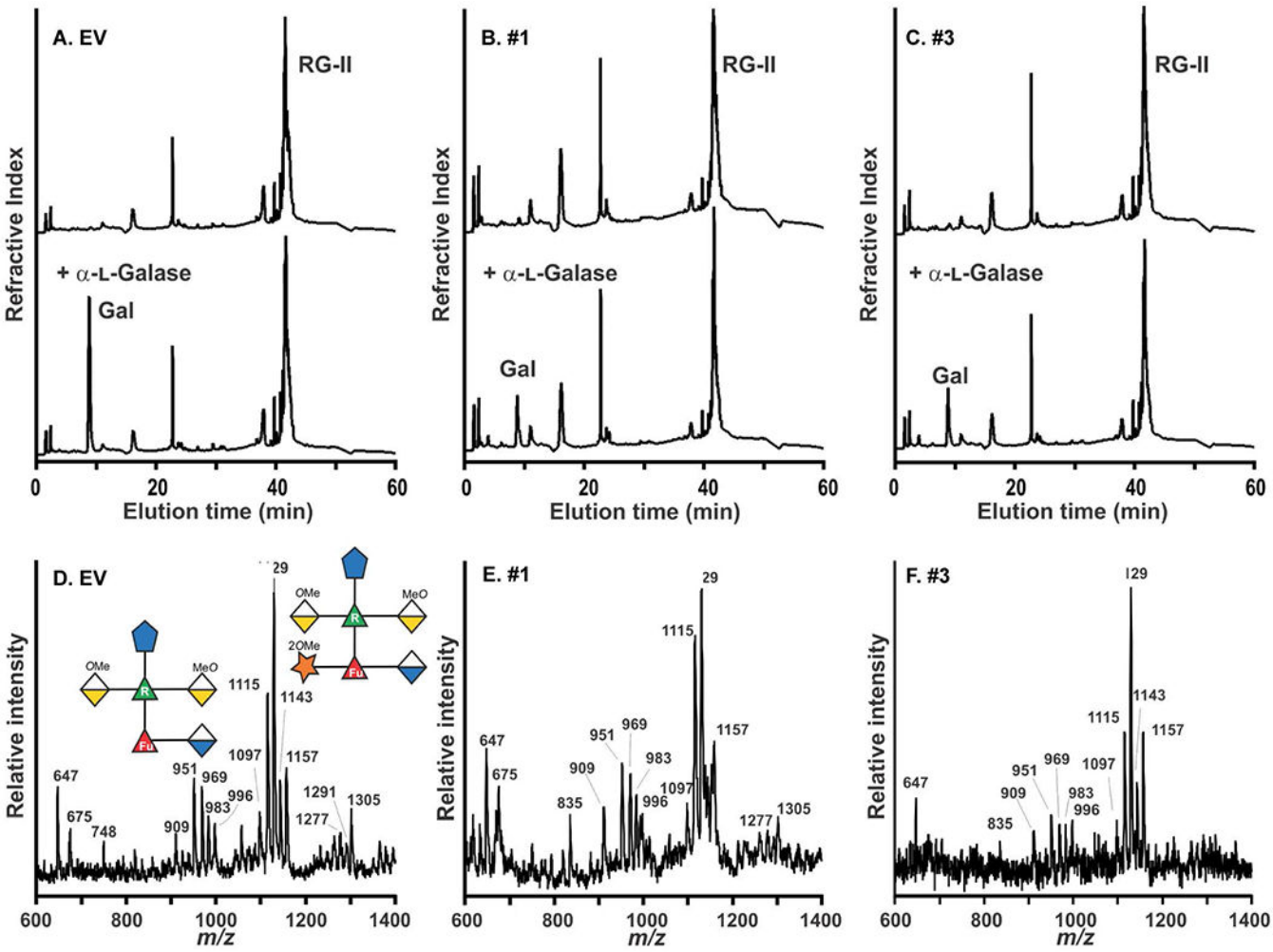

Figure 4: α-L-galactosidase treatment confirms that the RG-II from the hp*GGLT1* lines is deficient in α-L-galactose.

(A - C). The HPAEC-PAD profiles of untreated (top) and α-L-galactosidase-treated (bottom) RG-II from the EV control and h*pGGLT1* lines. The elution position of galactose, which was the only monosaccharide detected, is shown. (D – F) The negative ion MALDI-TOF mass spectrum of side-chain A generated by selective acid hydrolysis of L-galactosidase-treated RG-II. The predominant oligosaccharide (m/z 1115, 1129, 1143, and 1157) corresponds to side-chain A lacking L-galactose. The differences in mass of 14 Da correspond to differences in the extent of *O*-methylation of side-chain A. Only low intensity signals (m/z 1277, 1291, and 1305) corresponding to the L-galactose-containing side-chain A were detected. The oligosaccharides structures are represented using a modified SNFG nomenclature. See Figure 1 for details.

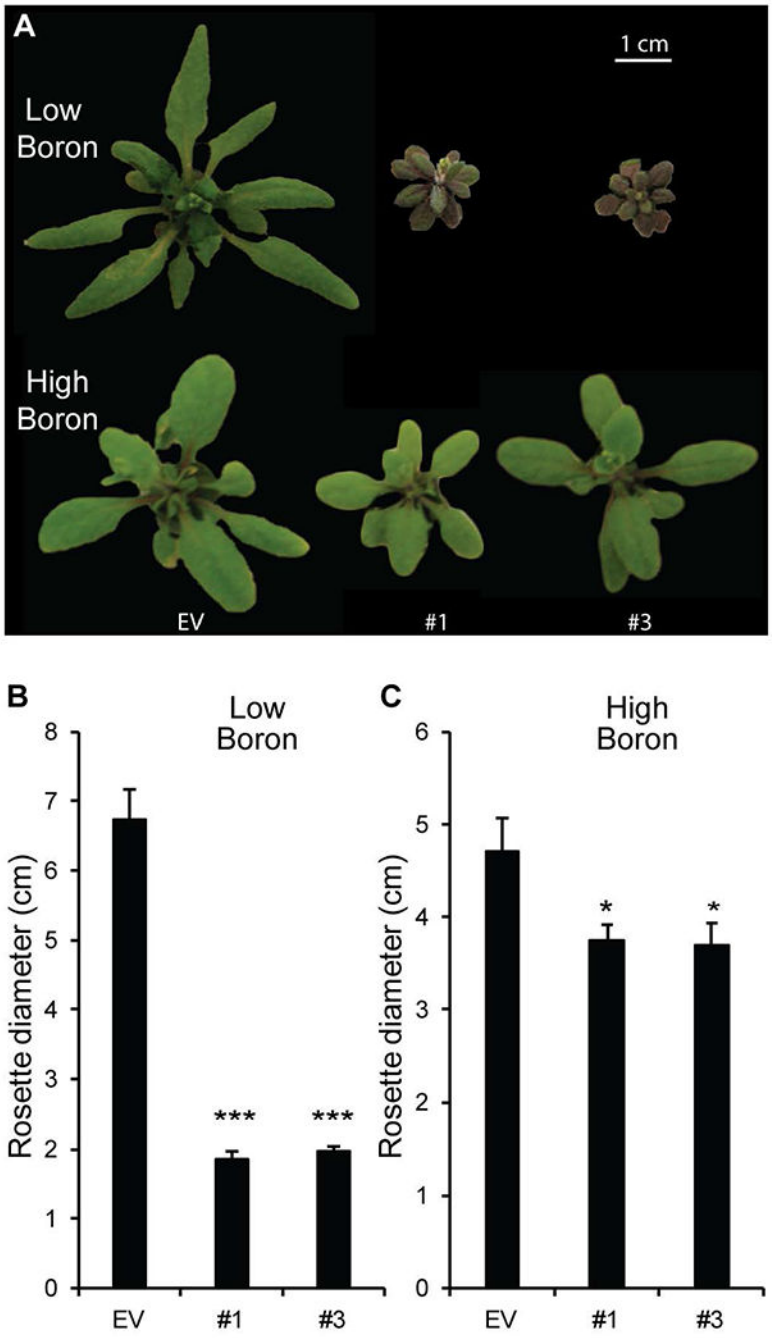

Figure 5: Boron complements hp*GGLT1* phenotypes.

Seeds were germinated on agar containing 1/2 MS (which contains 50 μM boric acid) and then grown for 7 days. The seedlings were then transferred to hydroponic growth media containing no added boric acid (low, 0 mM) or 1 mM boric acid (high boron). (A) Representative rosettes of 4-week-old plants. Quantification of rosette diameter in low boron (B) or high boron (C). The data for (B) and (C) represent the mean of 19-25 plants ± SEM. Asterisks indicate a significant different from EV (Student's t-test, * $P < 0.05$, ** $P < 0.01$, *** $P < 0.001$).

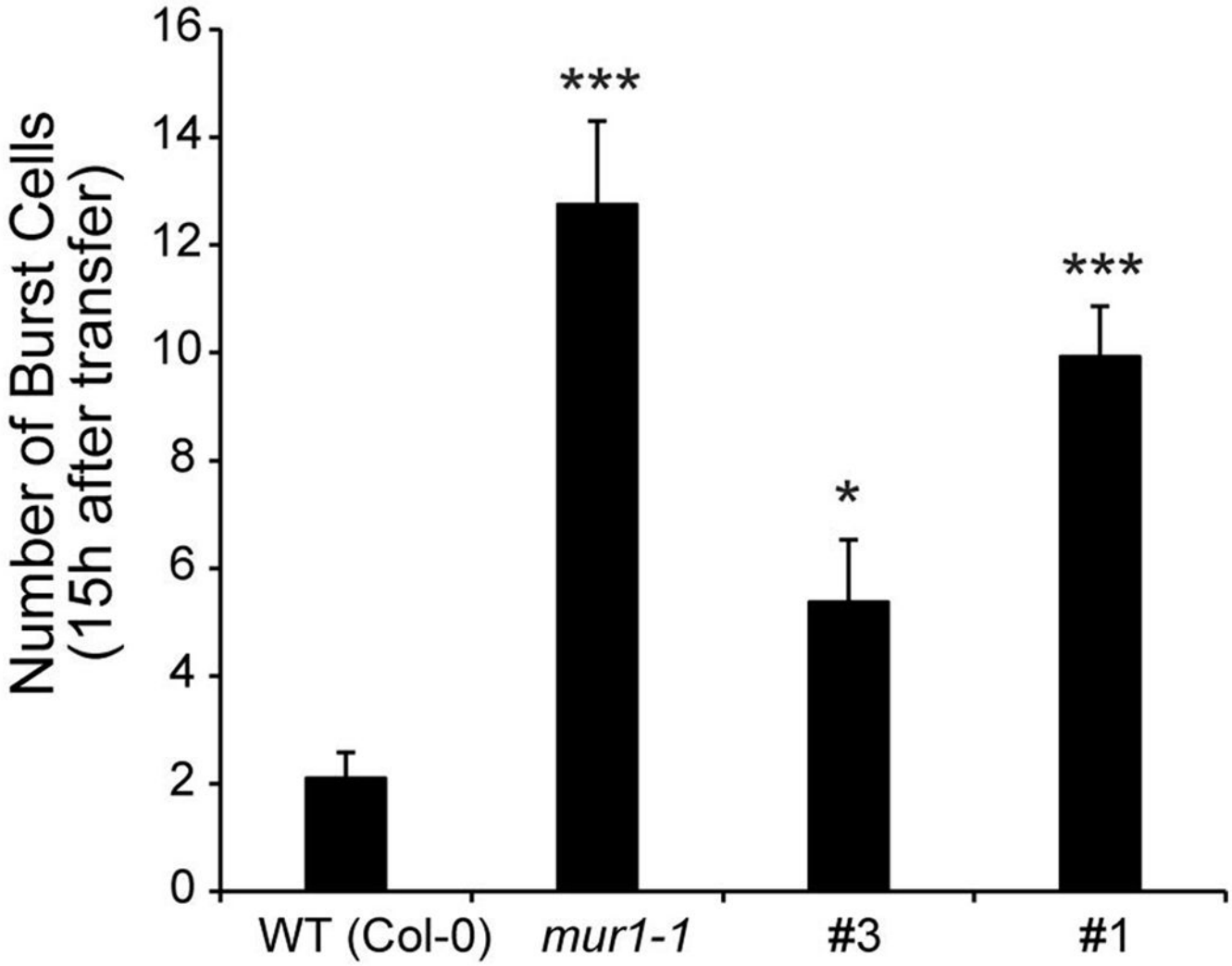

Figure 6: hp*GGLT1* roots display cell bursting during salt stress.

(A) Number of burst cells observed within the first 15h after salt treatment in WT, *mur1* and two *hpGGLT1* lines. (B) Representative time-lapse images of WT, *mur1* and *hpGGLT1* roots after salt treatment. The data for (A) represents the mean of 8-13 plants ± SEM. Asterisks indicate a significant different from WT (Student's t-test, * $P < 0.05$, ** $P < 0.01$, *** $P < 0.001$).

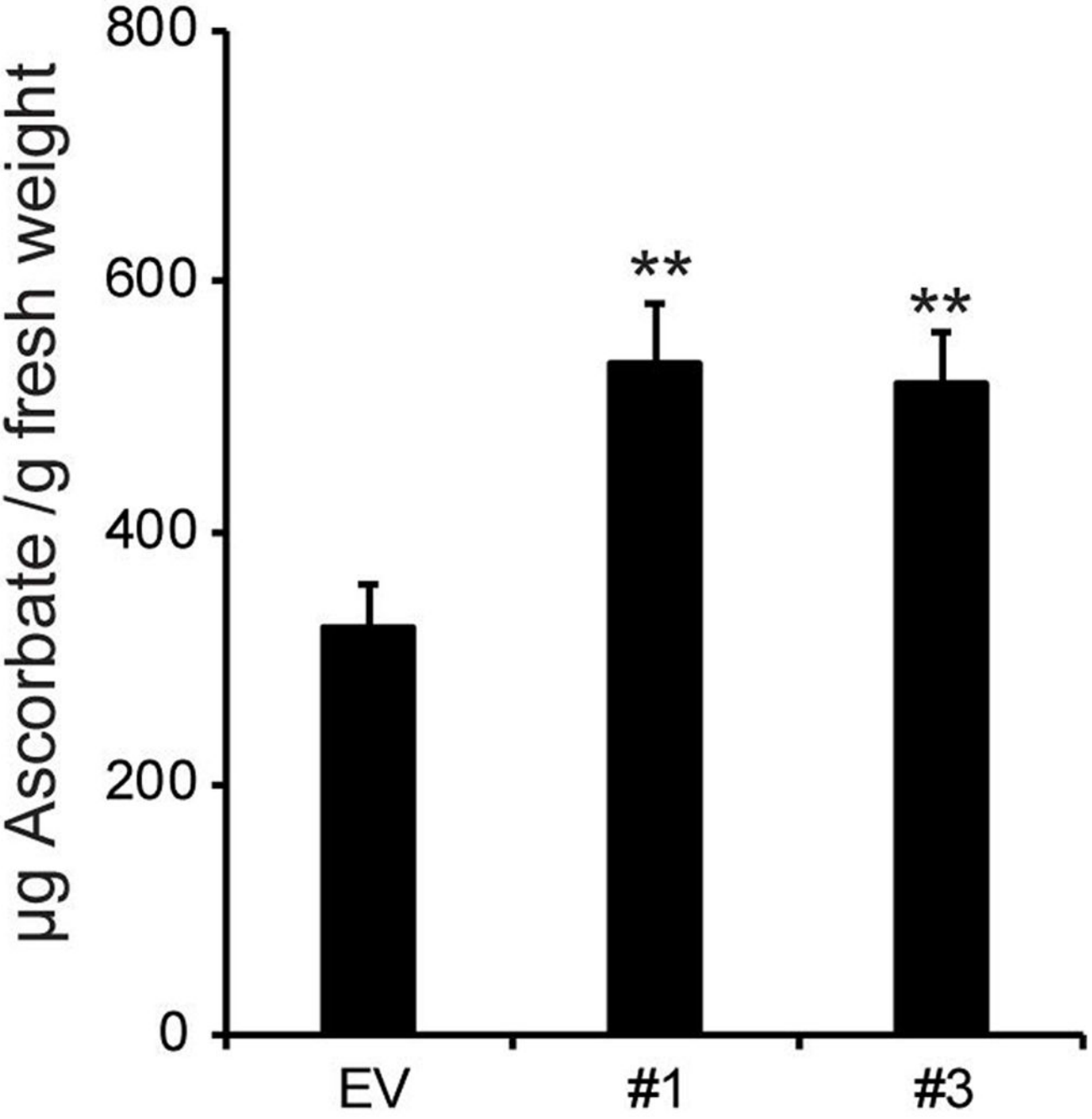

Figure 7: Ascorbic acid content of hp*GGLT1* leaves.

Data are the mean of 8-9 plants ± SEM. Asterisks indicate a significant different from EV (Student's t-test, * P < 0.05, ** P < 0.01, *** P < 0.001).

Table 1:
Monosaccharide composition of RG-II isolated from hp*GGLT1* plants.

RG-II was isolated by SEC and then hydrolyzed with TFA. The monosaccharides released were determined by HPAEC-PAD and by gas-liquid chromatography, and are presented as mol%.

	EV	#1	#3
MeFuc	4	4	4
Fuc	4	4	5
Rha	15	16	15
Ara	14	15	13
MeXyl	4	4	4
Api	9	10	10
AceA	3	3	4
Gal	15	9	10
GalA	29	32	31
GlcA	3	3	4